



Contents lists available at ScienceDirect

International Journal of Rock Mechanics and Mining Sciences

journal homepage: www.elsevier.com/locate/ijrmms

Estimation of pore microstructure by using the static and dynamic moduli

Lin Zhang^a, Jing Ba^{a,*}, Liyun Fu^b, José M. Carcione^c, Chenghao Cao^b

^a School of Earth Sciences and Engineering, Hohai University, Nanjing 211100, China

^b Institute of Geology and Geophysics, Chinese Academy of Sciences, Beijing 100029, China

^c Istituto Nazionale di Oceanografia e di Geofisica Sperimentale (OGS), Borgo Grotta Gigante 42c, Sgonico, Trieste I-34010, Italy

ABSTRACT

The variations of the static and dynamic moduli of porous rocks as a function of differential pressure have been described in terms of pore microstructure, i.e., the effects of cracks (soft pores) and intergranular (stiff) pores. Specifically, the first play a major role on the elastic properties of rocks. By using the Mori-Tanaka theory, this work relates rock elastic properties to the pore microstructure. Then, we estimate the distribution of pore aspect ratios by using the static bulk modulus instead of the dynamic one. The approach is applied to data from the Navajo and Weber sandstones. The results show that the cumulative crack porosity and density obtained from the static bulk modulus are higher than those estimated from the dynamic moduli, while the dominant crack aspect ratio is lower. The total porosity estimated from the static modulus agrees better with the experimental data. Furthermore, the cumulative crack (soft or compliant) porosity are estimated by the method, which also agrees with results from stress-strain relation and from bulk compressibility curves.

1. Introduction

The effects of pore microstructure on the static and dynamic stiffness moduli of rocks are important for evaluating reservoir properties.¹ Many works that study these effects are based on experimental ultrasonic velocities and static strain measurements.^{2–5} It has been found that the static and dynamic moduli greatly vary at low differential pressures ($P_d = P_c - P_p$, where P_c and P_p are the confining and pore pressures, respectively), a phenomenon that can be attributed to the opening of cracks when the pore pressure approaches the confining pressure. Izumotani and Onozuka⁶ stated that cracks with lower aspect ratio close first when the differential pressure increases and the ones with higher aspect ratios become thinner and then close under high pressure. The aspect ratio of a spheroidal crack is defined here as half the crack width divided by half the crack length and is always less or equal to one (a spherical pore in the latter case).

Essentially, the stress dependence of elastic properties is closely related to the pore microstructure. Walsh⁷ derived an expression of the elastic bulk modulus in dry rocks as a function of the confining pressure P_c (pore pressure is equal to zero). He found that the effect of the (compliant) cracks on the modulus is more significant than those of the intergranular (stiff) pores. In addition, Walsh⁷ estimated the crack porosity of the rock samples. Cheng and Toksöz⁸ obtained the porosity with different pore aspect ratios in sandstones by using the theory of Kuster and Toksöz.⁹ Other works which analyze the stiffness moduli variations with pressure are Berryman¹⁰ and Norris.¹¹ Shapiro¹² developed a relationship between the bulk compressibility and differential

pressure by dividing the total porosity ϕ into two parts: stiff porosity (ϕ_s) and compliant porosity (ϕ_c), and found that the compliant porosity (represented by the cracks) has a greater effect on the compressibility. Based on this theory, Pervukhina et al.¹³ analyzed experimental data and confirmed a linear dependence of the compressibility on the compliant porosity. Following these works, Han¹⁴ modeled the pressure dependence of velocity with a differential effective medium model and estimated the compliant pore aspect ratio. Accordingly, when the stress dependence of the elastic moduli is known, the distribution of pore aspect ratios can be estimated.

Since the Kuster and Toksöz⁹ theory fails to estimate the effective elastic moduli at high porosities, Tran et al.¹ modified the Cheng and Toksöz⁸ approach by introducing a differential effective medium (DEM) theory, and inverted the porosity from velocity data. However, their results are non-unique, and the reliability depends on the a-priori model. To solve this problem, Izumotani and Onozuka⁶ proposed a method for estimating the porosity with different aspect ratios by using very fast simulated annealing. Li et al.¹⁵ proposed a nonlinear global optimization algorithm to find the best effective pore aspect ratio. Similarly, Fortin et al.¹⁶ simulated the evolution of crack density and aspect ratio as a function of differential pressure in dry- and wet-rock specimens by using effective medium models.^{17,18}

Eberhart-Phillips et al.¹⁹ obtained an empirical relation between seismic velocity and pressure, based on a combination of linear and exponential terms. Zimmerman²⁰ used this relation to approximate the compressibility of three sandstone samples, and obtain their pore aspect ratio distributions. David and Zimmerman,²¹ hereafter called the DZ

* Corresponding author.

E-mail addresses: baj04@mails.tsinghua.edu.cn, jba@hhu.edu.cn (J. Ba).

<https://doi.org/10.1016/j.ijrmms.2018.11.005>

Received 13 May 2018; Received in revised form 4 November 2018; Accepted 11 November 2018

1365-1609/ © 2018 Elsevier Ltd. All rights reserved.

model, extended Zimmerman's²⁰ method to obtain a distribution of crack aspect ratios from dry-rock wave velocities, on the basis of the Mori-Tanaka theory,^{22,23} and predicted the wet-rock velocities as a function of differential pressure by using the Gassmann equations.^{24,25} Duan et al.²⁶ obtained the pore aspect ratio distribution of cracks in tight sandstones and analyzed the effects of cracks on wave dispersion and attenuation. Although these methods are easy to implement, their results generally are not in agreement with real data. It has been found that crack porosity is underestimated when predicted with the dynamic moduli (i.e., from wave velocities).^{8,13}

In this work, we propose the use of the static modulus instead of the dynamic modulus to obtain the crack porosity and density. First, we present the relations between elastic properties and pore structure based on the Mori-Tanaka theory.^{22,23} Thereafter, we derive an expression of the stress-strain relation based on the Zimmerman's²⁰ empirical relation and estimate the crack porosity from the static and dynamic moduli by using Walsh's⁷ method. Then, the DZ model is applied to the static modulus to estimate the distribution. The results are compared with those obtained from the dynamic moduli by using data for the Navajo and Weber sandstones.

2. Theoretical models

2.1. Relations between elastic properties and pore structure

Pore structure in rocks regards shape, volume concentration, distribution and connectivity of pores and cracks.⁸ Specifically, cracks have a major effect on elastic properties because they are compliant. In order to evaluate the effects of pore structure on elastic properties, effective medium theories are used to simulate an elastic isotropic material containing randomly-oriented stiff pores and compliant cracks. An expression for the effective compressibility C_{eff} under drained conditions (pore pressure is equal to zero, $P_c = P_d = p$) has been derived by Walsh,⁷ as follows:

$$C_{\text{eff}} = C_0 - \frac{d\phi}{dp}, \quad (1)$$

where $C_0 = 1/K_0$ is the bulk compressibility of the grains, ϕ is the total porosity and K_0 is the bulk modulus of the grains. Note that C_{eff} is related to the rate of change of porosity with pressure rather than porosity directly.

The approach assumes the pore system to be composed of stiff intergranular pores and compliant contacts/cracks. According to the Mori-Tanaka theory,^{22,23} the effective compliances of an isotropic solid comprising one family of randomly oriented spheroidal pores, are given by

$$C_{\text{stiff}} = C_0 \left(1 + \frac{\phi_{\text{stiff}}}{1 - \phi_{\text{stiff}}} P \right), \quad (2)$$

$$S_{\text{stiff}} = S_0 \left(1 + \frac{\phi_{\text{stiff}}}{1 - \phi_{\text{stiff}}} Q \right), \quad (3)$$

where $C_{\text{stiff}} = 1/K_{\text{stiff}}$, $S_{\text{stiff}} = 1/G_{\text{stiff}}$, and K_{stiff} and G_{stiff} are the bulk and shear moduli of the host material, respectively, ϕ_{stiff} is the stiff porosity and the shear compliance of the grains is $S_0 = 1/G_0$, where G_0 is the shear modulus, and P and Q are given by²⁷

$$P = \frac{(1 - \nu)}{6(1 - 2\nu)} \times \frac{4(1 + \nu) + 2\alpha^2(7 - 2\nu) - [3(1 + 4\nu) + 12\alpha^2(2 - \nu)]g}{2\alpha^2 + (1 - 4\alpha^2)g + (\alpha^2 - 1)(1 + \nu)g^2}. \quad (4)$$

$$Q = \frac{4(\alpha^2 - 1)(1 - \nu)}{15\{8(\nu - 1) + 2\alpha^2(3 - 4\nu) + [(7 - 8\nu) - 4\alpha^2(1 - 2\nu)]g\}} \times \left\{ \begin{array}{l} \frac{8(1 - \nu) + 2\alpha^2(3 + 4\nu) + [(8\nu - 1) - 4\alpha^2(5 + 2\nu)]g}{2\alpha^2 + (1 - 4\alpha^2)g + (\alpha^2 - 1)(1 + \nu)g^2} \\ - 3 \left[\frac{8(\nu - 1) + 2\alpha^2(5 - 4\nu) + [3(1 - 2\nu) + 6\alpha^2(\nu - 1)]g}{-2\alpha^2 + [(2 - \nu) + \alpha^2(1 + \nu)]g} \right] \end{array} \right\} \quad (5)$$

$$g = \begin{cases} \frac{\alpha}{(1 - \alpha^2)^{3/2}} (\arccos\alpha - \alpha\sqrt{1 - \alpha^2}) & (\alpha < 1) \\ \frac{\alpha}{(1 - \alpha^2)^{3/2}} (\alpha\sqrt{1 - \alpha^2} - \text{arccosh}\alpha) & (\alpha > 1) \end{cases} \quad (6)$$

where ν is Poisson's ratio of the grains, i.e., $\nu = (3K_0 - 2G_0)/(6K_0 + 2G_0)$, and α is the spheroidal aspect ratio.

Cracks are introduced into the host material using the Mori-Tanaka theory,^{22,23} neglecting the interaction between cracks and pores. It results in the following effective compliances for randomly oriented penny-shaped cracks:

$$C_{\text{eff}} = C_{\text{stiff}} \left(1 + \frac{16(1 - (v_{\text{stiff}})^2)\Gamma}{9(1 - 2v_{\text{stiff}})} \right), \quad (7)$$

$$S_{\text{eff}} = S_{\text{stiff}} \left(1 + \frac{32(1 - v_{\text{stiff}})(5 - v_{\text{stiff}})\Gamma}{45(2 - v_{\text{stiff}})} \right), \quad (8)$$

where $v_{\text{stiff}} = (3K_{\text{stiff}} - 2G_{\text{stiff}})/(6K_{\text{stiff}} + 2G_{\text{stiff}})$, and Γ is the crack density, given by

$$\Gamma = \frac{N\langle a^3 \rangle}{V}, \quad (9)$$

where a is the average radius of cracks and N is the total number of cracks embedded in a representative elementary volume V (the representative elementary volume has well-defined properties, such as porosity, permeability, and elastic moduli, which are representative of the medium). The brackets denote an average.

2.2. Analysis based on dry-rock experimental data

2.2.1. Estimation of crack porosity

Eq. (1) can be rewritten as

$$\frac{d\phi_c}{dp} = C_0 - C_{\text{eff}}. \quad (10)$$

Integrating between 0 and p_{close} , gives

$$\phi_c = \int_0^{p_{\text{close}}} C_{\text{eff}} dp - \int_0^{p_{\text{close}}} C_0 dp, \quad (11)$$

where p_{close} is the closure pressure of a pore, the first and second terms on the right-hand side are the areas A and B of the $C_{\text{eff}} - p$ and $C_0 - p$ curves, and the crack porosity ϕ_c is A-B, as shown in Fig. 1.

Eq. (11) can be rewritten as

$$\phi_c = \frac{\Delta V}{V} - C_0 p_{\text{close}}, \quad (12)$$

where ΔV is the decrease in volume V , and the crack porosity ϕ_c is the intercept on the volumetric strain axis as shown in Fig. 2.⁷

Hence, to compute the crack porosity, we need the relations between bulk compressibility (or strain) and stress. The issue has been discussed by many researchers.^{20,28} An empirical form of $C_{\text{eff}} - p$ is given by Zimmerman²⁰ as

$$C_{\text{eff}} = C_{\text{eff}}^{\text{hp}} + (C_{\text{eff}}^{\text{i}} - C_{\text{eff}}^{\text{hp}}) e^{-p/\hat{p}}. \quad (13)$$

Similarly,

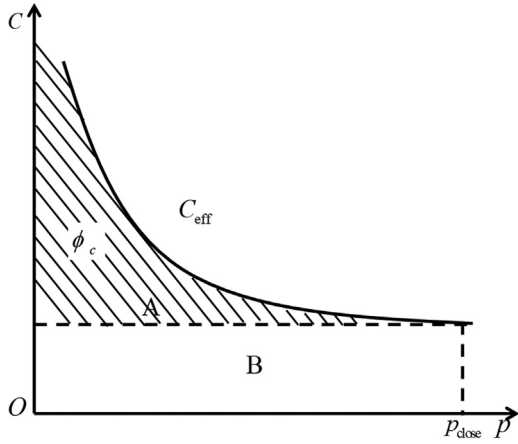


Fig. 1. Graphical determination of crack porosity from the $C_{\text{eff}} - p$ curve (see Eq. (11)).

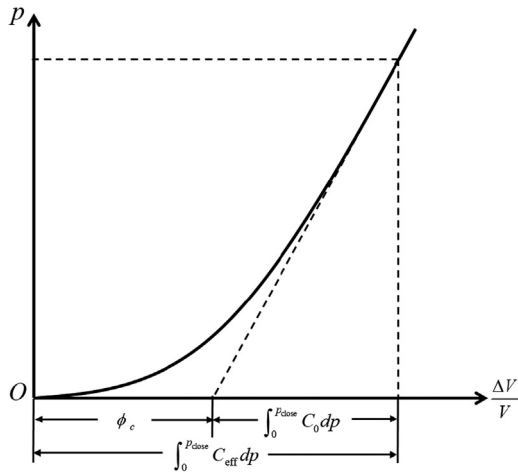


Fig. 2. Graphical determination of crack porosity from the $p - \Delta V/V$ curve (see Eq. (12)).

$$S_{\text{eff}} = S_{\text{eff}}^{\text{hp}} + (S_{\text{eff}}^{\text{i}} - S_{\text{eff}}^{\text{hp}})e^{-p/\hat{p}}, \quad (14)$$

where the superscript “hp” denotes the high-pressure value, the superscript “i” denotes the initial value (zero pressure), and the characteristic stress \hat{p} is a scaling factor, with dimension of pressure, that characterizes the rate at which the compliances level off.²⁰

By integrating Eq. (13) between 0 and p , we can get the stress-strain relation²⁰

$$\frac{\Delta V}{V} = C_{\text{eff}}^{\text{hp}} p + (C_{\text{eff}}^{\text{i}} - C_{\text{eff}}^{\text{hp}})\hat{p}(1 - e^{-p/\hat{p}}). \quad (15)$$

The crack porosity can be obtained from experimental data by fitting $\Delta V/V$ and velocities measured at different differential pressures.

2.2.2. Estimation of the pore aspect ratio distribution from the static bulk modulus

The pore-structure model (DZ) proposed by David and Zimmerman,²¹ which contains a distribution of cracks with different aspect ratios and stiff pores with a single aspect ratio, is used to invert the pore aspect ratio distribution. The modeling is performed in four steps as follows.

Step 1: Get the aspect ratio of the stiff pores. Since all the cracks are closed at high pressure, the effective elastic moduli of the host material are the high-pressure moduli. Hence, we can directly obtain the effective static bulk modulus $K_{\text{eff, st}}^{\text{hp}} = 1/C_{\text{eff, st}}^{\text{hp}}$ from the measured high-pressure bulk compressibility, or calculate its value from the high pressure

strain as

$$K_{\text{eff, st}}^{\text{hp}} = \frac{p}{\Delta V/V}. \quad (16)$$

Using Eq. (2), the aspect ratio $\alpha_{\text{st}}^{\text{hp}}$ can be obtained by a least-square regression of the high-pressure static bulk modulus.

Step 2: Calculate the cumulative crack density at each pressure. The pressure dependence of the effective moduli is closely related to the crack density. When the crack density is given, the elastic moduli can be obtained with Eqs. (7) and (8) and vice versa. Hence, we can calculate the value of the cumulative crack density $\Gamma_{p, \text{st}}(\alpha)$ by a least-square regression on the measured bulk modulus at each differential pressure p .

Step 3: Establish the relation between p and $\Gamma_{p, \text{st}}$. Step 2 only gives the crack density at each pressure p . Several researchers suggest that the change of crack density with pressure obeys an exponentially decay law,¹²

$$\Gamma_{p, \text{st}}(\alpha) = \Gamma_{\text{st}}^{\text{i}} e^{-p/\hat{p}}, \quad (17)$$

where $\Gamma_{\text{st}}^{\text{i}}$ is the initial crack density at zero differential pressure. Using the crack density at each pressure p , the fitting parameters in (17) can be calculated. Note that these parameters depend on the choice of the effective medium theory.

Step 4: Obtain the pore aspect ratio distribution. Denote with $\alpha_{\text{st}}^{\text{i}}$ and $\alpha_{\text{st}}(p)$ the crack aspect ratios at zero pressure and pressure p , respectively. At increasing differential pressure, cracks close and $\Gamma_{\text{st}}^{\text{i}}$ gradually decreases. All cracks open at pressure p have a minimum value of the initial aspect ratio $\alpha_{p, \text{st}}^{\text{i}}$, and according to David and Zimmerman²¹:

$$\alpha_{p, \text{st}}^{\text{i}} = \frac{3}{4\pi} \int_{\Gamma_{p, \text{st}}^{\text{i}}}^{\Gamma_{p, \text{st}}(\alpha)} \frac{(1/K_{\text{st}}(\Gamma_{p, \text{st}}) - 1/K_{\text{eff, st}}^{\text{hp}}) \hat{p}}{\Gamma_{p, \text{st}}} \frac{dp}{d\Gamma_{p, \text{st}}} d\Gamma, \quad (18)$$

where $K_{\text{st}}(\Gamma_p)$ is the effective static bulk modulus at pressure p given by Eq. (2).

Substituting Eq. (17) into (18), we obtain

$$\alpha_{p, \text{st}}^{\text{i}} = \frac{3}{4\pi} \int_{\Gamma_{p, \text{st}}^{\text{i}}}^{\Gamma_{p, \text{st}}(\alpha)} \frac{(1/K_{\text{st}}(\Gamma_{p, \text{st}}) - 1/K_{\text{eff, st}}^{\text{hp}}) \hat{p}}{\Gamma_{p, \text{st}}^2} d\Gamma_{p, \text{st}}. \quad (19)$$

Integrating Eq. (19) between Γ^{i} and $\Gamma_p(\alpha)$ yields

$$\alpha_{p, \text{st}}^{\text{i}} = \frac{4\hat{p}[1 - (\gamma_{\text{st}}^{\text{hp}})^2] \ln\left(\frac{\Gamma_{\text{st}}^{\text{i}}}{\Gamma_{p, \text{st}}(\alpha)}\right)}{3\pi K_{\text{eff, st}}^{\text{hp}} [1 - 2\gamma_{\text{st}}^{\text{hp}}]}, \quad (20)$$

where $\gamma_{\text{st}}^{\text{hp}} = (3K_{\text{eff, st}}^{\text{hp}} - 2G_{\text{eff, st}}^{\text{hp}})/(6K_{\text{eff, st}}^{\text{hp}} + 2G_{\text{eff, st}}^{\text{hp}})$ is the effective static Poisson ratio at high pressure

By combining Eqs. (17) and (20), the relation between aspect ratio and p is

$$\alpha_{p, \text{st}}^{\text{i}} = \frac{4[1 - (\gamma_{\text{st}}^{\text{hp}})^2] \hat{p}}{\pi E_{\text{st}}^{\text{hp}}}, \quad (21)$$

where $E_{\text{st}}^{\text{hp}}$ is the effective static Young modulus at high pressure and $E_{\text{st}}^{\text{hp}} = 3K_{\text{eff, st}}^{\text{hp}} [1 - 2\gamma_{\text{st}}^{\text{hp}}]$. Here, we assume that the decrease in aspect ratio is the same with an increment of differential pressure dp . Hence, when dp is small, the decrease in crack density is caused by cracks with aspect ratios smaller than $\alpha_{p, \text{st}}^{\text{i}}$. In this way, the pore aspect ratio distribution and the crack porosity at each pressure p are obtained from the experimental static bulk-moduli.

2.2.3. Estimation of the pore aspect ratio distribution from the dynamic moduli

By using the DZ model, we can extract the pore aspect ratio distribution from the P and S-wave velocities (V_p and V_s). The effective bulk and shear dynamic moduli, $K_{\text{dy}}^{\text{hp}}$ and $G_{\text{dy}}^{\text{hp}}$, are calculated by using the high-pressure wave velocities, as

$$K_{dy}^{hp} = \rho \left((V_p^{hp})^2 - \frac{4}{3} (V_s^{hp})^2 \right), \quad (22)$$

$$G_{dy}^{hp} = \rho (V_s^{hp})^2. \quad (23)$$

Then, steps 2–4 are the same of the previous section. As discussed by Pervukhina et al.,¹³ the difference between the static and dynamic moduli decreases with increasing differential pressure. This difference yields different values of pore aspect ratio distribution.

3. Results and discussion

Coyner⁴ provides velocities and static bulk moduli for two rocks, namely Navajo and Weber sandstones. The measurements were performed under dry conditions and up to a differential pressure of 100 MPa. The porosity of Navajo sandstone is 0.118 containing 89% quartz, 4% Kfeldspar, 4% illite, 2% kaolinite and 1% calcite.²⁹ Porosity is 0.095 for Weber sandstone and the mineral components are similar to Navajo sandstone.

3.1. Estimation of crack porosity from the stress-strain relation

On the basis of the equations given in Section 2.2.1, the crack porosity for the Navajo and Weber sandstones estimated from the stress-strain curves are shown in Fig. 3. For Navajo sandstone, the solid fitting curve is $\Delta V/V = 0.0489p + 0.0007(1 - e^{-p/0.014})$, where p is given in GPa, the goodness of the fit is $R^2 = 0.9998$ and the estimated crack porosity is 0.079%. For Weber sandstone, the solid fitting curve is $\Delta V/V = 0.0563p + 0.0059(1 - e^{-p/0.011})$, the goodness of the fit is $R^2 = 0.9999$ and the estimated crack porosity is 0.58%.

The data shows that both sandstones exhibit nonlinearity of the stress-strain curves, which is associated to the presence of cracks. The sensitivity is considered to be approximately inversely proportional to the aspect ratio of the cracks.^{12,30} Hence, the larger the sensitivity and the crack porosity, the more nonlinear is the stress-strain curve.

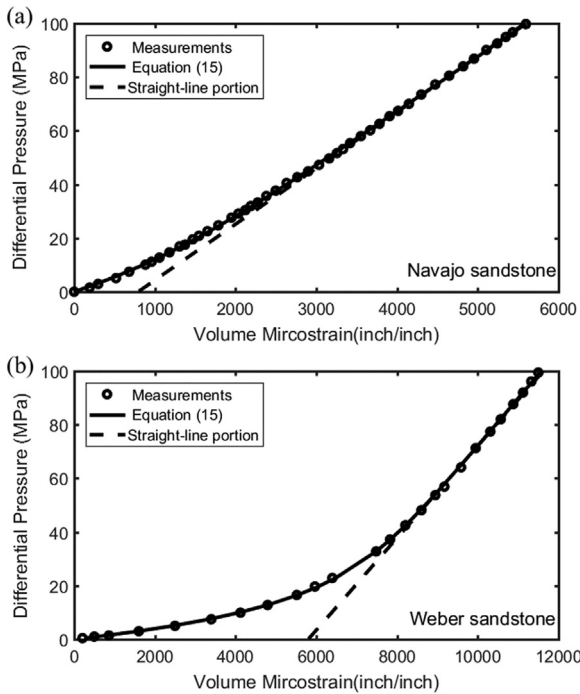


Fig. 3. Stress-strain curves for Navajo and Weber sandstones. The solid curve represents the fit with Eq. (15). The black circles are Coyner⁴ measurements. The broken curve is the stress-strain relation extrapolated to zero pressure.

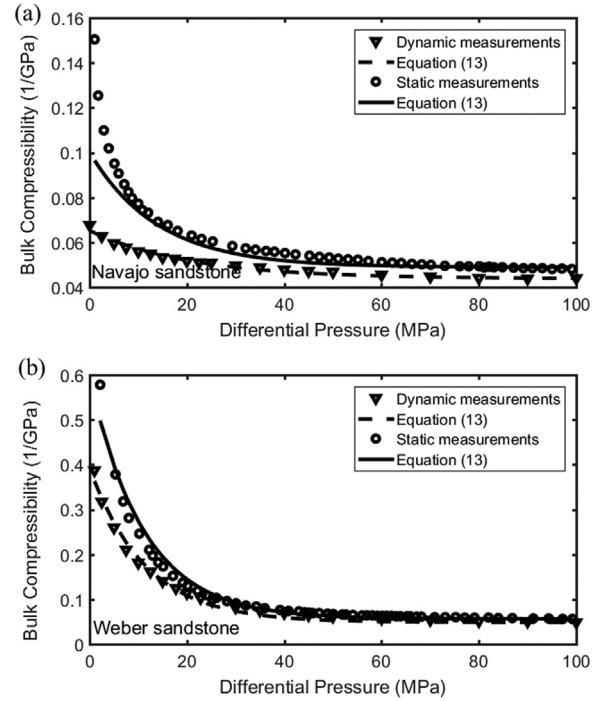


Fig. 4. Static (solid curve) and dynamic (broken curve) bulk compressibilities as a function of differential pressure for Navajo and Weber sandstones. The curve represents the fit with Eq. (13). The circles and triangles are Coyner⁴ measurements.

3.2. Estimation of the crack porosity from bulk compressibility

Experimental measurements of the static and dynamic bulk compressibilities of the two sandstones are shown in Fig. 4. As discussed in Section 2.2, if the relation between stress and strain (or wave velocities) is known, the expressions of the static (dynamic) bulk compressibility can be derived. The fit is shown in Table 1. For Navajo sandstone, the estimated crack porosity is 0.079% by using the static bulk compressibility, which is same of that estimated from the stress-strain curve, and $C_{eff,st}^{hp} = 0.0489 \text{ GPa}^{-1}$ and $C_{eff,st}^i = 0.0989 \text{ GPa}^{-1}$. Instead, the estimated crack porosity for Navajo Sandstone is 0.044% by using the dynamic bulk compressibility, and $C_{eff,dy}^{hp} = 0.0438 \text{ GPa}^{-1}$ and $C_{eff,dy}^i = 0.0652 \text{ GPa}^{-1}$. For Weber sandstone, the estimated “static” crack porosity is the same of that obtained with the stress-strain curves, i.e., 0.58%, with $C_{eff,st}^{hp} = 0.0563 \text{ GPa}^{-1}$ and $C_{eff,st}^i = 1.0994 \text{ GPa}^{-1}$. On the other hand, the estimated crack porosity is 0.25% by using dynamic bulk compressibility, with $C_{eff,dy}^{hp} = 0.0484 \text{ GPa}^{-1}$ and $C_{eff,dy}^i = 0.3924 \text{ GPa}^{-1}$. Then, these results indicate that static measurements yield a more consistent inversion of the crack porosity.

The results of Table 1 indicate that there is a higher fitting error in Fig. 4a for Navajo sandstone compared to Weber sandstone (Fig. 4b). The static bulk compressibility is approximately twice the dynamic bulk compressibility at low differential pressures. The difference decreases with increasing differential pressure. The estimated crack porosity from the static compressibility is higher than that obtained from the dynamic compressibility.

3.3. Estimation of the pore aspect ratio distribution

The closure pressure of a pore is $p_{close} = \pi E_0 \alpha_0 / (4(1 - (v_0)^2))$,⁷ where $E_0 = 3K_0(1 - 2v_0)$ is the Young modulus of the grains, and α_0 is the aspect ratio at $p = 0$. In a typical sandstone ($E_0 \sim 50 \text{ GPa}$), the closure pressure of a pore with an aspect ratio $\alpha = 0.01$ equals 500 MPa, which is far beyond the pressure used in the laboratory measurements. Hence, the aspect ratio of stiff pores can be considered in the range of

Table 1
Fitting parameters for the pressure dependence of the static and dynamic bulk compressibility.

Sandstone	$C_{eff,st}$	R^2	$C_{eff,dy}$	R^2
Navajo	$0.0489 + 0.05e^{-p/0.014}$	0.8	$0.0438 + 0.0214e^{-p/0.0208}$	0.9806
Weber	$0.0563 + 0.5364e^{-p/0.0111}$	0.9743	$0.0484 + 0.344e^{-p/0.0115}$	0.9896

Table 2
Inversion of the aspect ratio at high differential pressure.

Sandstone	α_{dy}^{hp}	Error on (V_p^{hp}, V_s^{hp})	α_{st}^{hp}	Error on ($K_{eff,st}^{hp}$)
Navajo	0.28	0.07%	0.18	0.09%
Weber	0.11	0.7%	0.08	0.99%

$0.01 < \alpha < 1$ and the aspect ratio of compliant cracks is less than 0.01.²¹

As discussed in Step 1 (Section 2.2.2), the aspect ratio of stiff pores are computed at high differential pressure, which are shown in Table 2. We have used $K_0 = 30$ GPa and $G_0 = 33$ GPa, calculated with a Voigt-Reuss-Hill average. The elastic properties of the minerals are taken from Mavko et al.³¹ These results show that the estimated aspect ratios from the dynamic moduli (wave velocities) are higher than those obtained from the static bulk modulus. In addition, as shown in Fig. 4, the dynamic bulk modulus approaches the static one at high pressure, and α_{dy}^{hp} also approaches α_{st}^{hp} .

The P- and S-wave velocities as a function of the differential pressure for Navajo sandstone are shown in Fig. 5. At low differential pressures, where cracks begin to close, the velocity sharply increases. This behavior is consistent with that reported in the literature.^{32–36} On the other hand, Fig. 6 gives the P- and S-wave velocities as a function of differential pressure for Weber sandstone, where a similar behavior can be observed.

Next, we obtain the pressure dependence of the crack density (Step 3 in Section 2.2.2). For Navajo sandstone, the static crack density is $\Gamma_{p,st} = 0.8842e^{-p/0.0089}$, with a goodness fit $R^2 = 0.9509$, and the dynamic

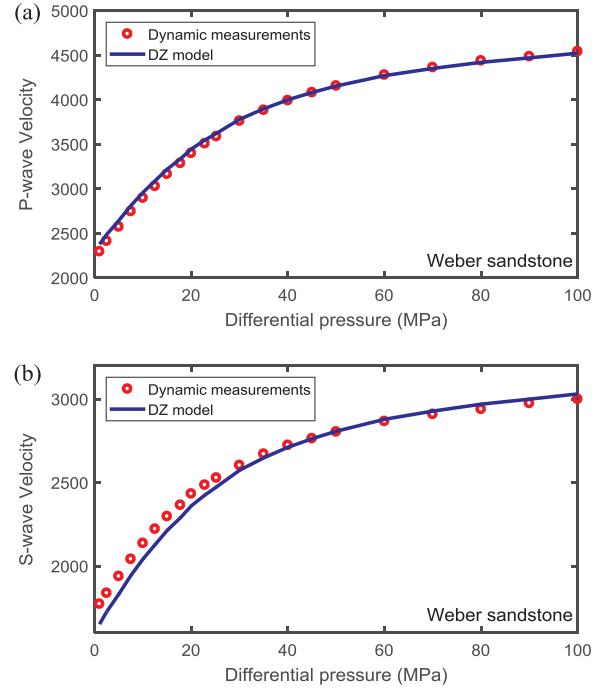


Fig. 6. P- and S-wave velocities as a function of differential pressure for Weber sandstone. The solid curve is the fit with the DZ model and the circles are Coyner⁴ measurements.

crack density is $\Gamma_{p,dy} = 0.2007e^{-p/0.0237}$, with a goodness fit $R^2 = 0.9894$. For Weber sandstone, the static crack density is $\Gamma_{p,dy} = 5.1001e^{-p/0.0089}$, with a goodness fit $R^2 = 0.9887$, and the dynamic crack density is $\Gamma_{p,dy} = 1.4596e^{-p/0.0154}$, with a goodness fit $R^2 = 0.9951$.

Following Step 4 (Section 2.2.2), the pore aspect ratio distribution is given in Fig. 7 for Navajo and Weber sandstones, where the broken and solid curves are obtained with dynamic and static data, respectively. It is evident that the whole crack porosity with different aspect ratios estimated from the static bulk modulus is higher than that estimated from the dynamic moduli. The “static” dominant porosity and aspect ratio are 0.00035% and 0.00023 for Navajo sandstone and 0.0023% and 0.00026 for Weber sandstone, respectively. The corresponding “dynamic” values are $7 \times 10^{-5}\%$ and 0.0006 (Navajo sandstone) and $6 \times 10^{-4}\%$ and 0.00045 (Weber sandstone). Both sandstones can be characterized by a bimodal porosity system, i.e. cracks and stiff pores. In previous studies, two constant aspect ratios have been used for modeling the pressure dependency of dynamic moduli with effective medium theories.^{14,37} In addition, the distributions of aspect ratio from dynamic moduli are found to be slightly wider than the static ones, which implies that the static moduli change is sharper due to the closure of the dominant cracks (see Fig. 7).

The results of the cumulative crack porosity and density are given in Fig. 8 and 9 for Navajo and Weber sandstones, respectively. According to the DZ model, when the cumulative crack porosity reaches an asymptotic value, the crack porosity can be estimated. Here, the cumulative crack porosity of Navajo sandstone estimated from the static bulk modulus is 0.084% and the cumulative crack density is 0.88, while the crack porosity from dynamic data is 0.047% and the crack density is 0.2. For Weber sandstone, the cumulative crack porosity estimated from

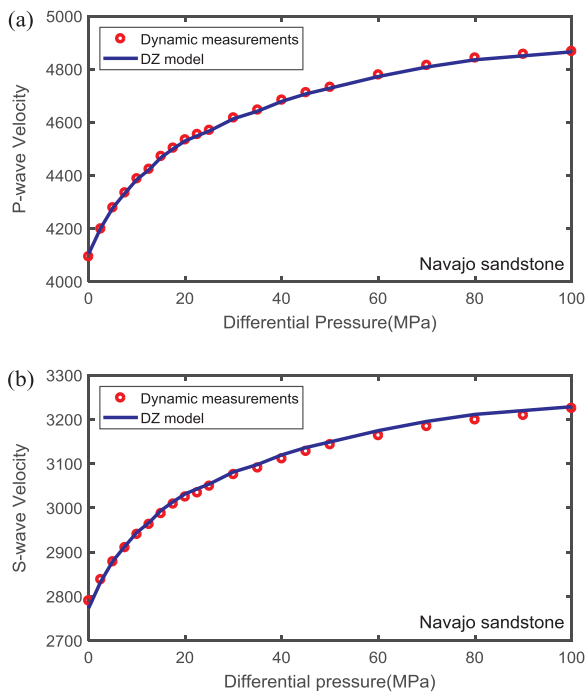


Fig. 5. P- and S-wave velocities as a function of differential pressure for Navajo sandstone. The solid curve is the fit with the DZ model and the circles are Coyner⁴ measurements.

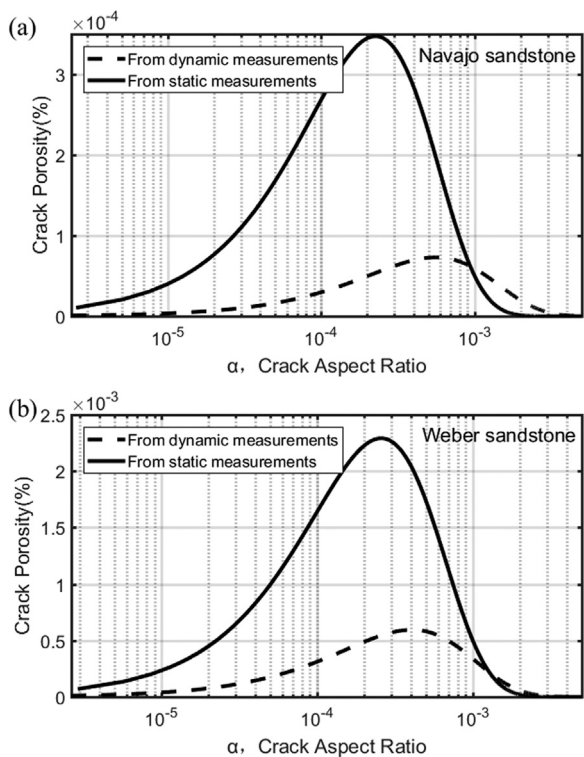


Fig. 7. Crack porosity as a function of crack aspect ratio for Navajo and Weber sandstones.

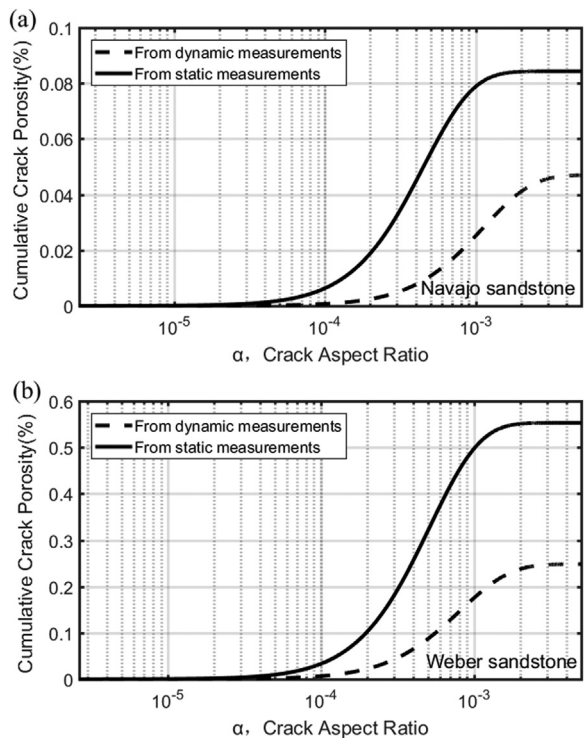


Fig. 8. Cumulative crack porosity as a function of crack aspect ratio for Navajo and Weber sandstones.

the static bulk modulus is 0.55% and the cumulative crack density is 5.1, while the crack porosity from dynamic data is 0.25% and the crack density is 1.5. The results show that although the estimated porosities are different by using the different methods, the values are within a reasonable range. The cumulative crack porosity and density estimated

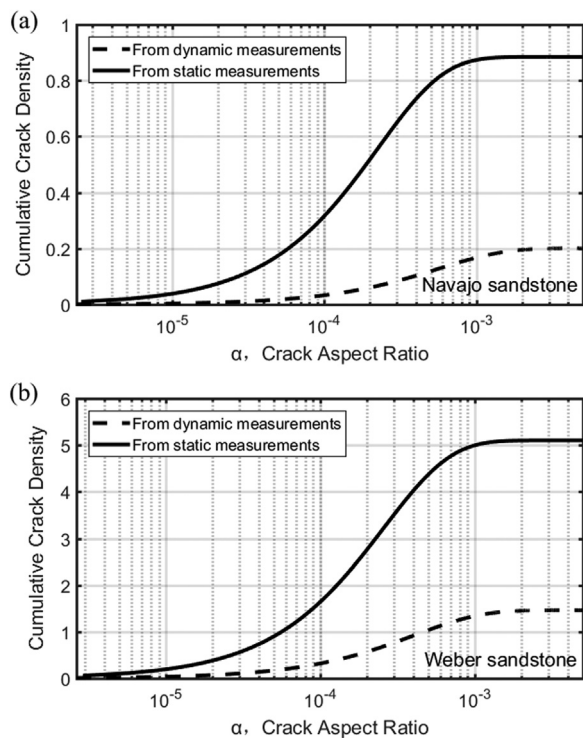


Fig. 9. Cumulative crack density as a function of crack aspect ratio for Navajo and Weber sandstones.

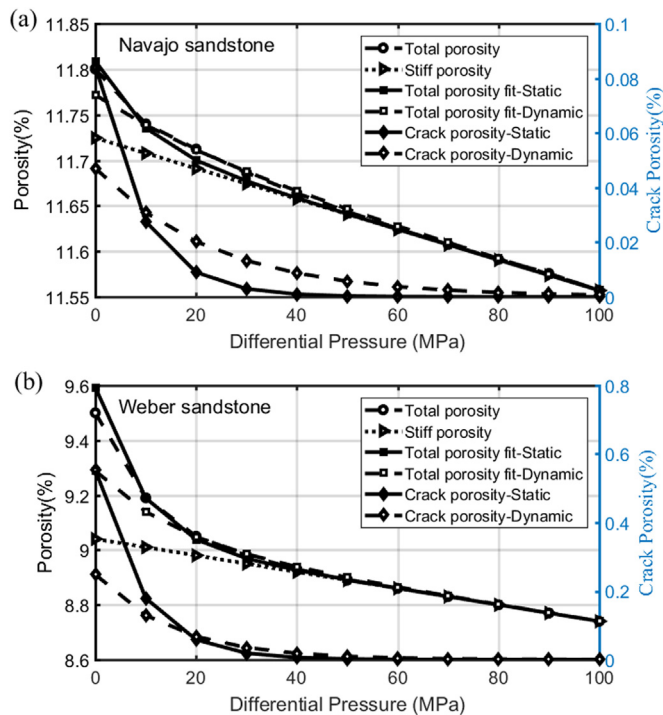


Fig. 10. Total, stiff and crack porosities as a function of differential pressure for Navajo and Weber sandstones. The broken line with circles denotes Coyner's⁴ measurements, the dotted line with triangles denotes the stiff porosity, the solid and broken lines with diamonds denote the crack porosities from static and dynamic data, respectively, and the line with squares denotes the fitting curve of the total porosity based on Pervukhina et al.¹³.

from the static bulk modulus are higher than those obtained from dynamic data.

The total, stiff and crack porosities of the two rocks as a function of

differential pressure are given in Fig. 10. The stiff porosity is estimated by a linear extrapolation of the high differential pressure data (dotted line with triangles).¹³ For Navajo sandstone, the pressure-dependent total porosity from static data has a correlation coefficient of $R^2 = 0.9933$, while the dynamic one is $R^2 = 0.9849$. For Weber sandstone, the correlation coefficients are 0.9820 and 0.9038, respectively. Moreover, the cumulative stiff porosities of Navajo and Weber sandstones are 11.72% and 9.04%, respectively. Then, the results show that the crack porosity estimated from the static bulk modulus better fits the data.

The relation between stiffness and differential pressure used by Zimmerman,²⁰ properly calibrated with experimental data, can be used to obtain the stress dependence of the elastic moduli and acoustic properties at different saturations, including full saturation conditions.³² This relation is very useful to model the mechanical deformations and seismic properties of rocks.

4. Conclusions

We have related the rock elastic properties to the pore microstructure by using the Mori-Tanaka theory. The stress-strain relation (Eq. (15)) has been validated with experimental data of Navajo and Weber sandstones. Then, a method for estimating the distribution of aspect ratios from the static bulk modulus is proposed, which is based on a technique previously used for dynamic moduli. We have obtained the crack porosity, density and aspect ratio distribution for two sandstones from static and dynamic measurements. It is worth noting that the crack porosity estimated from the static bulk compressibility is higher than that obtained from dynamic data, which validates the conclusion that the crack porosity estimated from dynamic moduli is an underestimation of the true porosity of rocks. This is due to the fact that the dynamic moduli calculated from ultrasonic measurements are higher than the static ones derived from stress-dependent porosity variations. Lower values of dynamic stress sensitivity compared to the static ones reflect the slower increment of dynamic moduli with pressure compared to static experiments. The difference is important at low differential pressures, where the static bulk compressibility can exceed the dynamic one by a factor of two. The method proposed here allows for a detailed characterization of pore structures in rocks, and it can also be used to analyze the relation between fabric textures and elastic properties.

Acknowledgements

We are very grateful to Prof. Emmanuel C. David from University College London for his valuable suggestion on this study. This work is supported by the Distinguished Professor Program of Jiangsu Province, the Cultivation Program of “111” Plan of China (Grant number: BC2018019) and the Fundamental Research Funds for the Central Universities (Grant number: 2016B13114). Data associated with this article can be accessed by contacting Jing Ba at jba@hhu.edu.cn.

References

- Tran DT, Rai CS, Sondergeld CH. Changes in crack aspect-ratio concentration from heat treatment: a comparison between velocity inversion and experimental data. *Geophysics*. 2008;71:E123–E132.
- King MS. Wave velocities in rocks as a function of changes in overburden pressure and pore fluid saturants. *Geophysics*. 1966;31(1):50–73.
- Nur A, Simmons G. The effect of saturation on velocity in low porosity rocks. *Earth Planet Sci Lett*. 1969;7(2):183–193.
- Coyner KB. *Effects of Stress, Pore Pressure, and Pore Fluids on Bulk Strain, Velocity, and Permeability in Rocks [Ph.D. dissertation]*. Massachusetts Institute of Technology; 1984.
- Baud P, Exner U, Lommatzsch M, Reuschlé T, Wong TF. Mechanical behavior, failure mode, and transport properties in a porous carbonate. *J Geophys Res: Solid Earth*. 2017;122(9):7363–7387.
- Izumotani S, Onozuka S. Elastic moduli and the aspect ratio spectrum of rock using simulated annealing. *Geophys Prospect*. 2013;61(s1):489–504.
- Walsh JB. The effect of cracks on the compressibility of rocks. *J Geophys Res*. 1965;70:381–389.
- Cheng CH, Toksöz MN. Inversion of seismic velocities for the pore aspect ratio spectrum of a rock. *J Geophys Res: Solid Earth*. 1979;84:7533–7543.
- Kuster GT, Toksöz MN. Velocity and attenuation of seismic waves in two-phase media: part I. Theoretical formulations. *Geophysics*. 1974;39:587–606.
- Berryman JG. Long wavelength propagation in composite elastic media II. Ellipsoidal inclusions. *J Acoust Soc Am*. 1980;68:1820–1831.
- Norris AN. A differential scheme for the effective moduli of composites. *Mech Mater*. 1985;4:1–16.
- Shapiro SA. Elastic piezosensitivity of porous and fractured rocks. *Geophysics*. 2003;68:482–486.
- Pervukhina M, Gurevich B, Dewhurst DN, Siggins AF. Applicability of velocity-stress relationships based on the dual porosity concept to isotropic porous rocks. *Geophys J Int*. 2010;181:1473–1479.
- Han T. A simple way to model the pressure dependency of rock velocity. *Tectonophysics*. 2016;675(Supplement C):1–6.
- Li HB, Zhang JJ, Yao FC. Inversion of effective pore aspect ratios for porous rocks and its applications. *Chin J Geophys*. 2013;56(2):608–615.
- Fortin J, Guéguen Y, Schubnel A. Effects of pore collapse and grain crushing on ultrasonic velocities and V_p/V_s . *J Geophys Res: Solid Earth*. 2007;112:B08207.
- Kachanov M. Elastic solids with many cracks and related problems. *Adv Appl Mech*. 1993;30:259–445.
- Shapiro B, Kachanov M. Materials with fluid-filled pores of various shapes: effective elastic properties and fluid pressure polarization. *Int J Solids Struct*. 1997;34:3517–3540.
- Eberhart-Phillips D, Han D-H, Zoback MD. Empirical relationships among seismic velocity, effective pressure, porosity and clay content in sandstone. *Geophysics*. 1989;54(1):82–89.
- Zimmerman RW. *Compressibility of Sandstones*. Amsterdam: Elsevier; 1991.
- David EC, Zimmerman RW. Pore structure model for elastic wave velocities in fluid-saturated sandstones. *J Geophys Res: Solid Earth*. 2012;117:B07210.
- Mori T, Tanaka K. Average stress in matrix and average elastic energy of materials with misfitting inclusions. *Acta Mater*. 1973;21:571–574.
- Benveniste Y. A new approach to the application of Mori-Tanaka's theory in composite materials. *Mech Mater*. 1987;6:147–157.
- Gassmann F. *Über die Elastizität poröser Medien: Vierteljahrsschrift der Naturforschenden Gesellschaft in Zürich*. 1951; 1951:1–23.
- Carcione JM. *Wave Fields in Real Media: Theory and numerical simulation of wave propagation in anisotropic, anelastic, porous and electromagnetic Media*. 3rd ed., extended and revised Elsevier; 2014.
- Duan C, Deng J, Li Y, Lu Y, Tang Z, Wang X. Effect of pore structure on the dispersion and attenuation of fluid-saturated tight sandstones. *J Geophys Eng*. 2018;15(2):449.
- David EC, Zimmerman RW. Compressibility and shear compliance of spheroidal pores: exact derivation via the Eshelby tensor, and asymptotic expressions in limiting cases. *Int J Solids Struct*. 2011;48:680–688.
- Liu HH, Rutqvist J, Berryman JG. On the relationship between stress and elastic strain for porous and fractured rock. *Int J Rock Mech Min Sci*. 2009;46:289–296.
- Parry WT, Forster CB, Evans JP, Bowen BB, Chan MA. Geochemistry of CO_2 sequestration in the Jurassic Navajo Sandstone, Colorado Plateau, Utah. *Environ Geosci*. 2007;14:91–109.
- Shapiro SA. Stress impact on elastic anisotropy of triclinic porous and fractured rocks. *J Geophys Res: Solid Earth*. 2017;122:2034–2053.
- Mavko G, Mukerji T, Dvorkin J. *The Rock Physics Handbook*. Cambridge: Cambridge University Press; 2009.
- Carcione JM, Helbig K, Helle HB. Effects of pressure and saturating fluid on wave velocity and attenuation of anisotropic rocks. *Int J Rock Mech Min Sci*. 2003;40:389–403.
- Agersborg R, Johansen TA, Jakobsen M, Sothcott J, Best A. Effects of fluids and dual-pore systems on pressure-dependent velocities and attenuations in carbonates. *Geophysics*. 2008;73:N35–N47.
- Han T, Best AI, Sothcott J, MacGregor LM. Pressure effects on the joint elastic-electrical properties of reservoir sandstones. *Geophys Prospect*. 2011;59:506–517.
- Asef MR, Najibi AR. The effect of confining pressure on elastic wave velocities and dynamic to static young's modulus ratio. *Geophysics*. 2013;78(3):D135–D142.
- Yurikov A, Lebedev M, Pervukhina M. Ultrasonic velocity measurements on thin rock samples: experiment and numerical modeling. *Geophysics*. 2017;83(2):1–40.
- Glubokovskikh Stanislav, Gurevich Boris, Saxena Nishank. A dual-porosity scheme for fluid/solid substitution. *Geophys Prospect*. 2016;64.4:1112–1121.